AFRL-RX-WP-TP-2009-4214

LASER-DEPOSITED CARBON NANOTUBE REINFORCED NICKEL MATRIX COMPOSITES (PREPRINT)

J. Tiley, J.Y. Hwang, A. Neira, T.W. Scharf, and R. Banerjee

Metals Branch
Metals, Ceramics and NDE Division

FEBRUARY 2008

STINFO COPY

AIR FORCE RESEARCH LABORATORY
MATERIALS AND MANUFACTURING DIRECTORATE
WRIGHT-PATTERSON AIR FORCE BASE, OH 45433-7750
AIR FORCE MATERIEL COMMAND
UNITED STATES AIR FORCE

REPORT DOCUMENTATION PAGE

1. REPORT DATE *(DD-MM-YY)*	2. REPORT TYPE	3. DATES COVERED *(From - To)*
February 2008	Journal Article Preprint	01 February 2008 – 01 February 2008

4. TITLE AND SUBTITLE	5a. CONTRACT NUMBER
LASER-DEPOSITED CARBON NANOTUBE REINFORCED NICKEL MATRIX COMPOSITES (PREPRINT)	In-house
	5b. GRANT NUMBER
	5c. PROGRAM ELEMENT NUMBER 62102F

6. AUTHOR(S)	
J. Tiley (AFRL/RXLMN)	**5d. PROJECT NUMBER** 4347
J.Y. Hwang, A. Neira, T.W. Scharf, and R. Banerjee (The University of North Texas)	**5e. TASK NUMBER** RG
	5f. WORK UNIT NUMBER M02R1000

7. PERFORMING ORGANIZATION NAME(S) AND ADDRESS(ES)		8. PERFORMING ORGANIZATION REPORT NUMBER
Metals Branch (RXLMN) Metals, Ceramics and NDE Division Materials and Manufacturing Directorate Wright-Patterson Air Force Base, OH 45433-7750 Air Force Materiel Command, United States Air Force	Department of Materials Science and Engineering The University of North Texas Denton, TX	AFRL-RX-WP-TP-2009-4214

9. SPONSORING/MONITORING AGENCY NAME(S) AND ADDRESS(ES)	10. SPONSORING/MONITORING AGENCY ACRONYM(S)
Air Force Research Laboratory Materials and Manufacturing Directorate Wright-Patterson Air Force Base, OH 45433-7750 Air Force Materiel Command United States Air Force	AFRL/RXLMD
	11. SPONSORING/MONITORING AGENCY REPORT NUMBER(S) AFRL-RX-WP-TP-2009-4214

12. DISTRIBUTION/AVAILABILITY STATEMENT
Approved for public release; distribution unlimited.

13. SUPPLEMENTARY NOTES
To be submitted to Scripta Materialia
PAO Case Number and clearance date: WPAFB 08-0496, 25 February 2008.
This is the best copy available.
The U.S. Government is joint author of this work and has the right to use, modify, reproduce, release, perform, display, or disclose the work.

14. ABSTRACT
Composites based on multi-walled carbon nanotubes dispersed in nickel matrix have been processed using the laser-engineered net shape technique. The present study focuses on the survival of nanotubes in liquid nickel matrix during melt processing. The stability of nanotubes versus graphite powders in liquid nickel has been compared by processing both types of composites under identical conditions and subsequently characterizing their microstructure and chemical stability in detail using scanning and transmission electron microscopy, and micro-Raman spectroscopy.

15. SUBJECT TERMS
Ni-based nanocomposite, laser deposition, metal matrix composite, carbon nanotube, interface

16. SECURITY CLASSIFICATION OF:			17. LIMITATION OF ABSTRACT:	18. NUMBER OF PAGES	19a. NAME OF RESPONSIBLE PERSON (Monitor)
a. REPORT Unclassified	**b. ABSTRACT** Unclassified	**c. THIS PAGE** Unclassified	SAR	24	Christopher F. Woodward **19b. TELEPHONE NUMBER** *(Include Area Code)* N/A

i

1
2
3
4
5
6
7
8
9
10
11
12
13
14
15
16
17
18
19
20
21
22
23
24
25
26
27
28
29
30
31
32
33
34
35
36
37
38
39
40
41
42
43
44
45
46
47
48
49
50
51
52
53
54
55
56
57
58
59
60
61
62
63
64
65

Laser-deposited Carbon Nanotube Reinforced Nickel Matrix Composites

J. Y. Hwang, A. Neira, T. W. Scharf, J. Tiley*, and, R. Banerjee

Department of Materials Science and Engineering, The University of North Texas, Denton, Texas, USA
*Air Force Research Laboratory, Materials and Manufacturing Directorate, WPAFB, Ohio, USA

Abstract

Composites based on multi-walled carbon nanotubes dispersed in nickel matrix have been processed using the laser-engineered net shape technique. The present study focuses on the survival of nanotubes in liquid nickel matrix during melt processing. The stability of nanotubes versus graphite powders in liquid nickel has been compared by processing both types of composites under identical conditions and subsequently characterizing their microstructure and chemical stability in detail using scanning and transmisison electron microscopy, and micro-Raman spectroscopy.

Keywords: Ni-based nanocomposite; Laser deposition; Metal matrix composite; Carbon nanotube; Interface

Introduction

Nanocomposites based on carbon nanotubes (CNT) in metal matrices offer attractive properties such as high strength, stiffness, as well as enhanced electrical and thermal properties [1-3], and are therefore of interest for aerospace applications. Among the large number of potential application proposed, the application of CNTs as reinforcements in matrices holds the most promise for engineering applications. While a huge volume of research activities have focused on polymer matrices reinforced with CNTs [4], there have been relatively fewer studies carried out on metal matrices reinforced with nanotubes. Furthermore, in many cases, metal/CNT composites have not shown promising results due to the difficulties associated with processing these nanocomposites, especially in terms of achieving a homogenous distribution of the CNTs and associated with interfacial reactions between the metal matrix. In terms of distribution of

1

nanotubes in a metal matrix, the most promising results appear to be those reported using a molecular level mixing process [1]. While this processing technique has led to very uniform distributions of individual (to a cluster of few) multi-walled carbon nanotubes (MWCNTs) in metal matrices such as copper, the ability to scale up such a process for large scale production has to be demonstrated. Other processing techniques, more capable of producing larger quantities of nanotube reinforced metal-matrix composites include, thermal spraying as well as sintering and consolidation of mechanically milled powders. Thus, MWCNT reinforced Al alloy nanocomposites have been successfully processed by plasma spraying and high-velocity oxy fuel spraying techniques [2].

Recently, the issues of interfacial reaction between MWCNT and Al-based matrices have been discussed extensively [2,5-6], and have led to controversy in mechanical properties of these nanocomposites. Ci et al. report that the formation of an Al_4C_3 layer at the nanotube/matrix interface due to an interfacial reaction leads to better bonding between the nanotube and the Al matrix, and consequently an improvement in the mechanical properties of these nanocomposites [5]. However, Chunfeng et al. report that in 2024 Al alloy composites with MWCNTs, processed via a ball milling coupled with hot sintering (~ 873 K) technique, the nanotubes react completely with the Al based matrix and get converted to Al_4C_3 carbide precipitates leading to poorer mechanical properties [6]. The high reactivity of the MWCNTs with the Al based matrix has been attributed to the high energy ball milling involved in this processing route. In a different study on thermally sprayed nanocomposites based on Al-23wt%Si reinforced with MWCNTs, Laha et al. suggest that the Si in the matrix reacts preferentially with the carbon in the MWCNTs to form a β-SiC layer at the interface [2]. The formation of this interfacial reaction layer promotes the wettability and the interfacial adhesion in these nanocomposites. These papers raise important issues related to the role of interfacial reaction between nanotubes and metals.

It has been demonstrated that direct fabrication of metal matrix composites using the laser engineered net shaping (LENS™) process can lead to refined and homogeneous distribution of the reinforcement phase as well as deposit functionally graded materials [7-8]. Laser deposition using LENS™ involves a liquid metal processing route with a powder feedstock. Therefore, the motivation of the present paper is to explore the possibility of processing metal-matrix nanocomposites based on MWCNTs reinforcing a nickel matrix using LENS™ deposition. This study permits to investigate the interaction of MWCNTs with liquid

2

nickel as well as the survivability of such nanotubes during laser processing. In this context it is important to point out that previous research indicates that nickel exhibits good wettability for graphite powders [9]. Also, while liquid nickel exhibits substantially high solubility for carbon at high temperatures, solid nickel has negligible solubility for carbon at room temperature and nickel does not form an equilibrium carbide phase [10].

Experimental Procedure

The LENS™ process begins with a CAD design file, which is post-processed into a series of 2D layers. A 0.25" stainless steel substrate is used as a base for deposition. To provide the best build, each successive layer was deposited in a scan direction that was different from the previous layer to ensure homogeneity. A high pulsed Nd:YAG laser, emitting near-infrared laser radiation at a wavelength of 1.064 μm, is focused on the substrate to create a melt pool into which the powder feedstock is delivered through an inert gas flowing through a multi-nozzle assembly. The powders used in this study consisted of CP-Nickel (44 - 149μm near spherical particle size from Crucible Research™) and 5 wt% graphite powders (for the Ni + graphite composites) or 10 vol% MWCNT. The system specific control parameter included laser power of 400W (35Amp), hatch width of 0.25", layer thickness of 0.01", and mass flow rate of Ar in the powder feeders of 3.5 liters/min. The graphite powder particles are highly irregular in shape and their size ranged from 10 - 70 μm. Since the MWCNT used in this study were in the form of bundles consisting of multiple nanotubes coiled up within this bundle, it is rather difficult to determine the exact length of these nanotubes, even from TEM studies. Nevertheless, based on TEM observations of a few individual nanotubes which had separated from the bundles, the average length was found to be ~ 10 μm. The bundle size (or diameter) of the CNTs was in the range of 5 - 50 μm. Prior to deposition, the nickel and CNT (or graphite) powders were pre-mixed in a twin-roller mixer consisting of two rolls rotating in opposite directions (one clockwise and one anticlockwise). This mixing was carried out for 24 hours, immediately following which the pre-mixed powder was introduced into the power feeder of the LENS deposition system and the composites were laser deposited. Reducing the time between the end of the mixing process and the introduction of the pre-mixed powder into the power feeder and final deposition ensured minimal segregation in the powder feedstock due to the substantial density differences between

3

nickel and CNTs. Both the nickel + graphite as well as the nickel + CNT composites were LENS deposited in a cylindrical geometry of diameter ~ 10 mm and height ~ 10 mm.

The LENS™ deposited samples were sectioned using an abrasive cutting wheel and subsequently mounted and mechanically polished for metallographic observation. These samples were characterized using a FEI Quanta 200 scanning electron microscope. In order to study the details of the microstructure, site specific TEM sample was extracted from regions containing the nanotube/nickel matrix interface using a FEI Nova Nanolab 200, dual-beam focused ion beam (FIB) instrument. The TEM specimen was characterized in both a FEI/Phillips E-420, TEM and a FEI TECNAI F20 FEG-TEM operating at 120 kV and 200 kV respectively. In addition, site-specific micro Raman spectroscopy was carried out using a Thermo Electron Almega XR Dispersive Raman Spectrometer with ~1μm spot size and 532nm excitation wavelength. Raman spectra were obtained at a low power of 20 mW corresponding to a laser power density (~25 mW/μm^2); at this power density, no changes in the spectra due to laser surface heating could be seen. The acquisition times were 10 seconds/spectrum with 4 total accumulations taken to average each spectrum. Raman shifts were measured over a frequency range from 200 to 3000 cm^{-1}, with ~2 cm^{-1} resolution.

Results and Discussion

In order to investigate the stability of graphite powder in a liquid nickel bath during LENS™ deposition, a Ni + 5 wt% graphite composite was deposited. The pre-mixed initial powder feedstock, consisting of nickel and graphite powder particles, is shown in SEM image in Fig. 1(a). Backscatter SEM images showing the microstructure of the laser-deposited Ni/graphite composite are presented in Figs. 1(b) and (c). The as-deposited microstructure was comprised of primary graphite and a eutectic mixture of Ni + graphite. In some local regions of the deposit unmelted graphite powder particles were also observed. The primary graphite exhibited a globular shape with sizes ranging from ~ 2 - 10 μm, as shown in Fig. 1(b). Comparing Figs. 1(a) and (b), the difference between the primary graphite precipitates and the pre-mixed graphite powder particles is evident from their size scales and morphologies. Thus, the primary graphite precipitates in the LENS deposited composite are of a much finer scale and also exhibit a near spherical morphology. In addition to the primary graphite, there is also some finer scale eutectic

4

graphite present in the nickel matrix, as shown in Fig. 1(b). The Ni-C phase diagram exhibits a eutectic reaction at 1327°C with a small solubility of C ($\sim$ 1 wt%) in solid Ni at high temperatures ($\sim$ 1300°C) and almost negligible solubility of C in solid Ni at room temperature [10]. However, liquid Ni exhibits a large solubility for C. Furthermore, Ni does not form any equilibrium carbide phase. Based on the microstructural observations of the LENS™ deposited Ni/graphite composites, it can be concluded that during the deposition process, the larger irregular shaped graphite powder particles dissolved in the liquid Ni pool at high temperatures and on cooling re-precipitated as primary graphite and eutectic Ni + graphite. Therefore, under these laser deposition conditions, the graphite powder is not stable in the molten Ni pool.

An SEM image of the mixed nickel and MWCNT powders is shown in Fig. 2(a). The nickel powder particles are near spherical in this image and their size ranges from 50 – 150 μm. The CNTs are present in the form of non-spherical coarse bundles ranging in size from 5 – 50 μm. A higher magnification image of one such bundle of size $\sim$ 5 μm, clearly exhibiting agglomerated nanotubes, is shown as an inset in the same figure. A TEM image of agglomerated multi-walled nanotubes of $\sim$ 40-60 nm in diameter is shown in Fig. 2(b). A high resolution TEM image, shown as an inset in the same figure, clearly reveals the graphene sheets in the nanotube wall together with the hollow region shown in the bottom portion of this image. Fig. 3 shows backscatter SEM images of the microstructure of MWCNT reinforced Ni nanocomposites deposited by LENS™ using the same parameters as the Ni/graphite composites discussed in the previous section of this paper. Homogeneously distributed second phase particles are present in the nickel matrix (refer Fig. 3(a)). These second phase particles are near-spherical in morphology and range in diameter from 1 to 5 μm, as clearly visible in the higher magnification SEM image in Fig. 3(b). Chemical analysis of these bundles using energy dispersive spectroscopy (EDS) in the SEM indicated that these bundles contained a substantial amount of carbon. However, it is not possible to explicitly discern the identity of these bundles based solely on the SEM results. In order to investigate the structure of these bundles and the interface between the bundles and matrix, a site-specific TEM sample was prepared using the dual-beam FIB. Initially, the area adjacent to one of the bundles was protected by ion assisted Pt deposition and then the region of interest was milled. Fig. 4(a) shows the site-specific TEM sample during the milling process in the dual-beam FIB. A bright-field TEM image from this sample is shown in Fig. 4(b). In this TEM image, the region exhibiting the lighter contrast corresponds to the bundle while the region

5

exhibiting the darker contrast corresponds to the surrounding nickel matrix. Two different areas have been marked as I and II in Fig. 4(b). Regions I is located within the bundle while region II contains the interface between the bundle and the Ni matrix.

Higher magnification TEM images from these two different areas are shown in Fig. 5. Thus, Figs. 5(a), and (c), correspond to regions I and II respectively. Figs. 5(a) and (b) show distinct MWCNTs within the LENS deposited composite. While Fig. 5(a) shows a lower magnification bright-field TEM image of the CNTs in region I, Fig. 5(b) shows a high resolution TEM image of a section of the wall of one of the nanotubes, clearly exhibiting the graphene layers in the wall. A higher magnification image of the graphene layers in the wall is shown as an inset in Fig. 5(b). A selected area electron diffraction pattern from the nanotubes shown in Fig. 5(a), is shown in Fig. 5(d). This electron diffraction pattern can be consistently indexed based a nanotube structure comprising of multiple graphene sheets forming the wall of the nanotube. Fig. 5(c), corresponding to region II, shows the interface between the agglomerated MWCNTs in a bundle and the nickel matrix. This micrograph also shows clear evidence of nanotubes extending right up to the interface. Furthermore, while there appears to be wetting of the nanotubes by the nickel matrix, the interface appears to be sharp with no evidence of a reaction layer of any substantial thickness at this interface. The evidence for the presence of distinct nanotubes in this composite indicates that the agglomerated MWCNTs survived the laser-deposition process and did not dissolve in the molten nickel pool, which is a very distinct difference compared to Ni/graphite interaction. Though the graphite powders as well as the agglomerated MWCNTs (or bundles) exhibit similar sizes and melting temperatures, both materials do not behave the same way during LENS™ deposition. The interaction of both these forms of carbon with liquid nickel appears to be significantly different. Thus, while the graphite powder particles clearly dissolve in the liquid nickel, the MWCNTs do not dissolve in the molten nickel pool. The interface between the nickel and the agglomerated MWCNTs shows no significant evidence of interaction between two substances and consequently a sharp interface (refer to Fig. 5(c)). These observations suggest that the chemical stability of MWCNTs in the molten nickel pool is much better than that of the graphite powder particles. A possible scientific rationale for the higher stability of CNTs in the molten nickel pool as compared with the graphite power particles is that since the CNTs are rolled up graphene sheets, they have only the end carbon atoms with unsaturated covalent bonds and therefore the nanotubes are likely to react and dissolve only from the ends. In contrast,

the graphite powder particles consist of a large number of graphene sheets held together by weak Van der Waals bonds and consequently these particles can react easily and dissolve in the molten nickel pool.

Raman spectroscopy is particularly useful for studying carbon-based materials due to strong enhancement of Raman C-C band intensities, from the resonant Raman effect in the 1300 to 3000 cm^{-1} region, which often show changes in their peak location and intensity, depending on the structure of the carbon. Fig. 6 shows the micro-Raman spectra from the Ni/MWCNT nanocomposite sample. Three of the four spectra correspond to different sizes of the MWCNT bundles observed in the composite sample while the fourth one corresponds to the MWCNT powder used as a feedstock for the LENS™ deposition, and acts as a reference. All Raman spectra showed only carbon peaks present on the surface. The primary peaks observed in Fig. 6 are at ~ 1350, ~ 1580, and, ~ 1620 cm^{-1} wavenumbers, corresponding to the D, G, and, D′ peaks of the nanotubes, respectively [11]. In the reference sample, corresponding to pure MWCNTs, the G peak exhibits a substantially higher intensity as compared to the D peak. Also, the intensity of the D′ peak is very small and is seen as a shoulder to the primary G peak. With decreasing size of the MWCNT bundles from ~ 5μm to ~1μm, the intensity of the G peak relative to the D peak progressively decreases coupled with an increase in the intensity of the D′ peak. The intensities, wavenumbers and intensity ratio of the D, G, and D′ peaks for the different MWCNT bundles are listed in Table 1.

The D peak origin is due to the breathing modes of sp^2 bonded atoms in rings, the G peak is attributed to the in-plane bond stretching of all pairs of sp^2 bonded atoms in both rings and chains, and the D′ peak is a double resonance Raman band induced by defects [11-12]. The disorder, in a qualitative sense, in MWCNT can be monitored via the D and D′ peaks and their intensities are considered defect dependent, e.g. bond length and angle (curvature) disorder at the atomic scale. The I_D/I_G ratio has been often used to correlate the structural purity of graphitic materials to the graphite crystal domain size, L_a [13]. L_a can be considered as an average interdefect distance and one can still assume that the higher the number of defects, the higher the D peak intensity and, thus, the smaller L_a [12]. From Fig. 6 and Table 1, the main features in the Raman spectra of the MWCNT powder as well as different sized bundles in the LENS™ processed MWCNT composites are:

(a) G peak increases from 1572 to 1583 cm^{-1};

(b) D′ peak becomes more pronounced at ~1621 cm^{-1};

(c) I_D/I_G increases with reduction in bundle size

From the Raman parameters, two phenomena are evident, namely the change in defect density (increases with I_D/I_G) and the degree of graphitization (increases with higher shift of G peak). The first trend, when comparing the as-received MWCNT powder to the large size bundles (~5μm) in the laser-deposited MWCNT composite, is an increase in defect concentration (I_D/I_G changes from 0.20 to 0.32) while the G peak shifts in wavenumber from 1572 to 1583 cm^{-1} implying some graphitization during the laser deposition process. The second trend, when comparing different MWCNT bundle sizes, is the increase of I_D/I_G with decreasing bundle size, which indicates a higher number of defects with smaller domain (or bundle) sizes. This trend is further supported by the more pronounced D′ peak observed as a function of decreasing bundle size. No shift in the G peak position is exhibited when comparing Raman spectra from the different bundle sizes suggesting no change in graphitization.

The observed increase in the defect density of the CNTs with decreasing bundle size, as reflected by the increase in the I_D/I_G ratio in the micro-Raman spectra, can possibly be attributed to the interaction of the Nd:YAG laser beam (used in LENS deposition) with the CNTs. There have been previous reports on electron beam / CNT [14,15], ion beam / CNT [16], and laser / CNT [17] interactions. Thus, high energy electron irradiation (1.8 MeV) has been shown to have a substantial impact on the Raman vibrational spectra, depending on the dosage level [14]. In a separate study on electron irradiation effects on CNTs exposed to a less than 100 keV beam in a standard TEM, the authors conclude that prolonged exposures can cause severe damage of the nanotube structure [15]. In terms of ion irradiation, exposing CNTs to 21 keV Ag ion irradiation indicates that the graphene wall structure is retained for fluences upto 7×10^{13} ions/cm^2. However, the graphene wall structure was destroyed when exposed to higher fluences [16]. In a recent paper discussing the interaction of CNTs with an Nd:YAG laser beam during pulsed laser deposition (PLD) of MWCNT thin films, it was reported that there is minimal morphological damage of the nanotubes as well as structural changes induced due to the laser interaction [17]. The only observed change in the Raman spectra from these PLD deposited MWCNT thin films on alumina substrates was a slight shift and broadening of the Raman peaks associated with the substrate, suggesting some possible damage or stress induced in the substrate at locations where

8

the nanotubes are attached [17]. Based on these reported results, it appears that the influence of laser beam interactions with the CNTs is not well understood and further research work is warranted.

Summary and Conclusions

MWCNTs reinforced nickel matrix composites were deposited using the LENS™ processing technique. During the laser deposition process, while bundles of the CNTs retained their identity in the liquid nickel, graphite powders, deposited under similar conditions, dissolved in the liquid nickel and re-precipitated as primary and eutectic graphite. This suggests a higher stability of MWCNT bundles as compared with graphite powder, of similar size, during liquid melt processing. Furthermore, the degree of graphitization of the MWCNT bundles as well as their defect density increased during laser deposition. Within the MWCNT reinforced nickel matrix composite, the density of defects in the MWCNT bundles increased as the bundle size decreased.

Acknowledgements

Reference

[1] S. I. Cha, K. T. Kim, S. N. Arshad, C. B. Mo, S. H. Hong, Adv. Mater. 17 (2005) 1377.

[2] T. Laha, S. Kuchibhatla, S. Seal, W. Li, A. Agarwal, Acta Mater. 55 (2007) 1059.

[3] S. Yamanaka, A. Kawasaki, H. Sakamoto, Y. Mekuchi, M. Kuno, and, T. Tsukada, J. Jpn. Inst. Met. 70 (2006) 630.

[4] S. R. Bakshi, J. E. Tercero, A. Agarwal, Composites: Part A 38 (2007) 2493-2499.

[5] L. Ci, Z. Ryu, N. Y. Jin-Phillip, and, M. Rühle, Acta Mater. 54 (2006) 5367.

[6] D. Chunfeng, Z. Xuexi, and, W. Dezun, Mater. Lett. 61 (2007) 904.

[7] R. Banerjee, A. Genç, D. Hill, P. C. Collins, and H. L. Fraser, Scripta Mater. 53 (2005) 1433.

[8] R. Banerjee, P. C. Collins, D. Bhattacharyya, S. Banerjee, and H. L. Fraser, Acta Mater. 51 (2003) 3277.

[9] S. W. Ip, R. Sridhar, J. M. Toguri, T. F. Stephenson, and, A. E. M. Warner, Mater. Sci. Eng. A 244 (1998) 31.

[10] Alloy Phase Diagrams, ASM Handbook Vol. 3, ASM International, p. 533 (1992).

[11] K. Behler, S. Osswald, H. Ye, S. Dimovski, and Y. Gogotsi, J. Nanoparticle Res. 8 (2006).

[12] A.C. Ferrari, Solid State Commun. 143 (2007) 47.

[13] F. Tuinstra, and J.L. Koening, J. Chem. Phys. 53 (1970) 1126.

[14] U. Ritter, P. Scharff, C. Siegmund, O. P. Dmytrenko, N. P. Kulish, Yu. I. Prylutsky, N. M. Belyi, V. A. Gubanov, L. I. Komarova, S. V. Lizunova, V. G. Poroshin, V. V. Shlapatskaya, and, H. Bernas, Carbon, 44 (2006) 2694.

[15] K. Molhave, S. B. Gudnason, A. T. Pedersen, C. H. Clausen, A. Horsewell, and, P. Boggild, Ultramicroscopy, 108 (2007) 52.

[16] S. Mathew, U. M. Bhatta, B. Joseph, and, B. N. Dev, Nuc. Instr. Methods Phys. Res. B, 264 (2007) 36.

[17] F. Bonaccorso, C. Bongiorno, B. Fazio, P. G. Gucciardi, O. M. Marago, A. Morone, and, C. Spinella, Appl. Sur. Sci., 254 (2007) 1260.

Table

Bundle Size (μm)	I_D	D (cm^{-1})	I_G	G (cm^{-1})	I_D/I_G	D' (cm^{-1})
1	598	1349	494	1583	1.21	1621
3	840	1349	1349	1583	0.62	1621
5	702	1349	2224	1583	0.32	1621
MWNCT	646	1345	3218	1572	0.20	1617

Table 1. Raman D and G peak parameters for MWCNTs and different sizes of the MWCNT bundles observed in the composites.

Figure Captions

Fig. 1. (a) SEM image of pre-mixed nickel + graphite powders used for LENS deposition. (b) Backscatter SEM image showing the typical microstructure of the laser-deposited Ni/graphite composite. (c) Higher magnification SEM image of the eutectic region shown in (b).

Fig. 2. (a) SEM image of pre-mixed nickel + MWCNT powders used for LENS deposition. Inset shows a higher magnification image of a single MWCNT bundle. (b) TEM image of the raw MWCNTs. The HRTEM image as an inset shows the multi-walled graphene sheets and hollow region.

Fig. 3. (a) Backscatter SEM images of the laser-deposited MWCNTs reinforced Ni nanocomposite. (b) Higher magnification image of the same microstructure.

Fig. 4. (a) SEM image of a site-specific TEM sample during the milling process in the FIB. (b) Bright-field TEM image of the same specimen with regions I and II marked (see text for details).

Fig. 5. (a) Bright-field TEM image from region I (marked in Fig. 4(b)), showing nanotubes within a bundle in the LENS deposited composite. (b) High resolution TEM image of a section of the wall of one of these nanotubes with an inset showing the graphene structure. (c) TEM image of the nickel / CNT bundle interface. (d) SAD pattern taken from region I.

Fig. 6. Micro-Raman spectra of raw MWCNT and three different size of bundles from the Ni/MWCNT nanocomposite.
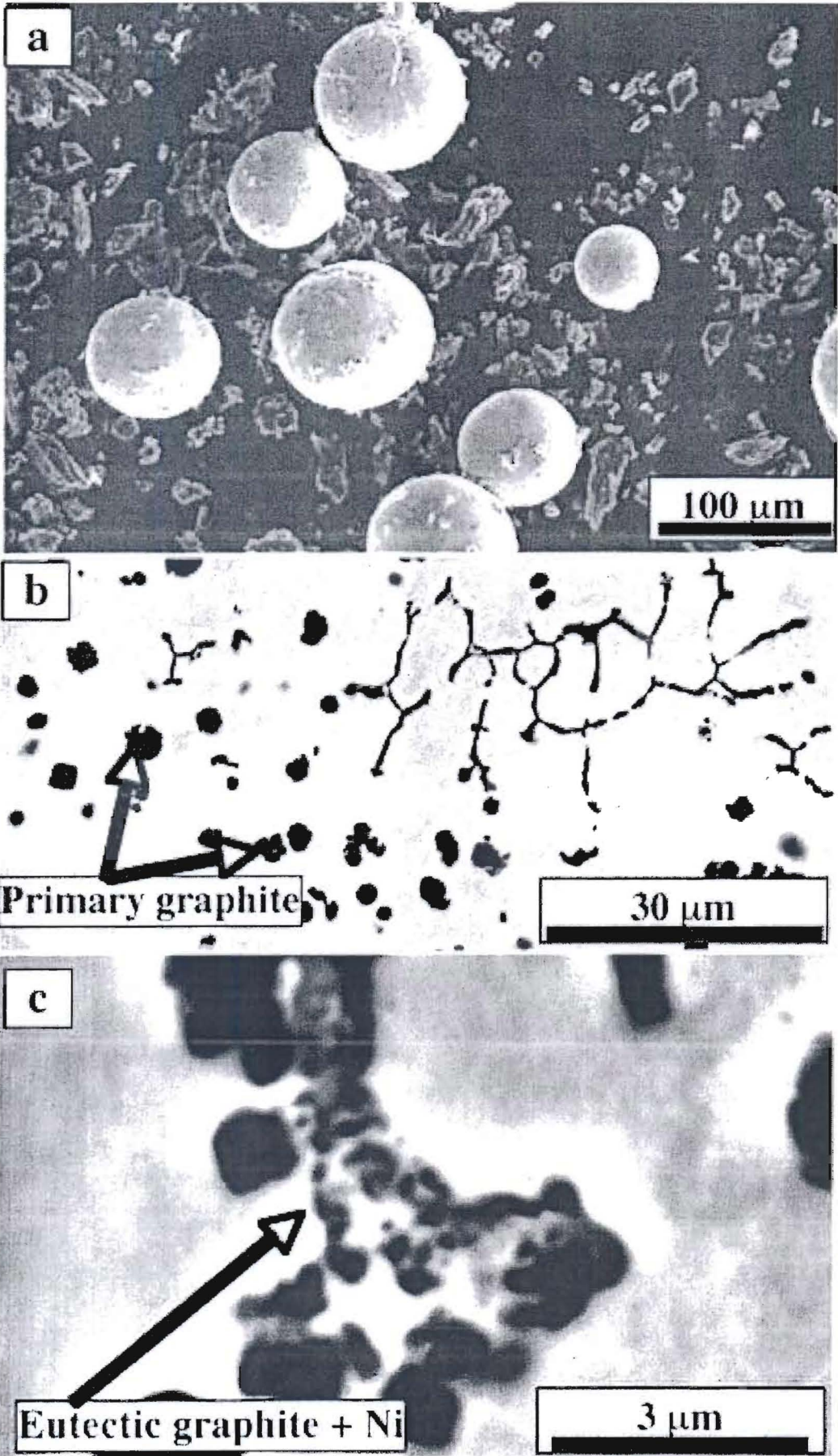
Figure 1
Click here to download high resolution image

a

100 μm

b

Primary graphite

30 μm

c

Eutectic graphite + Ni

3 μm

Figure 2
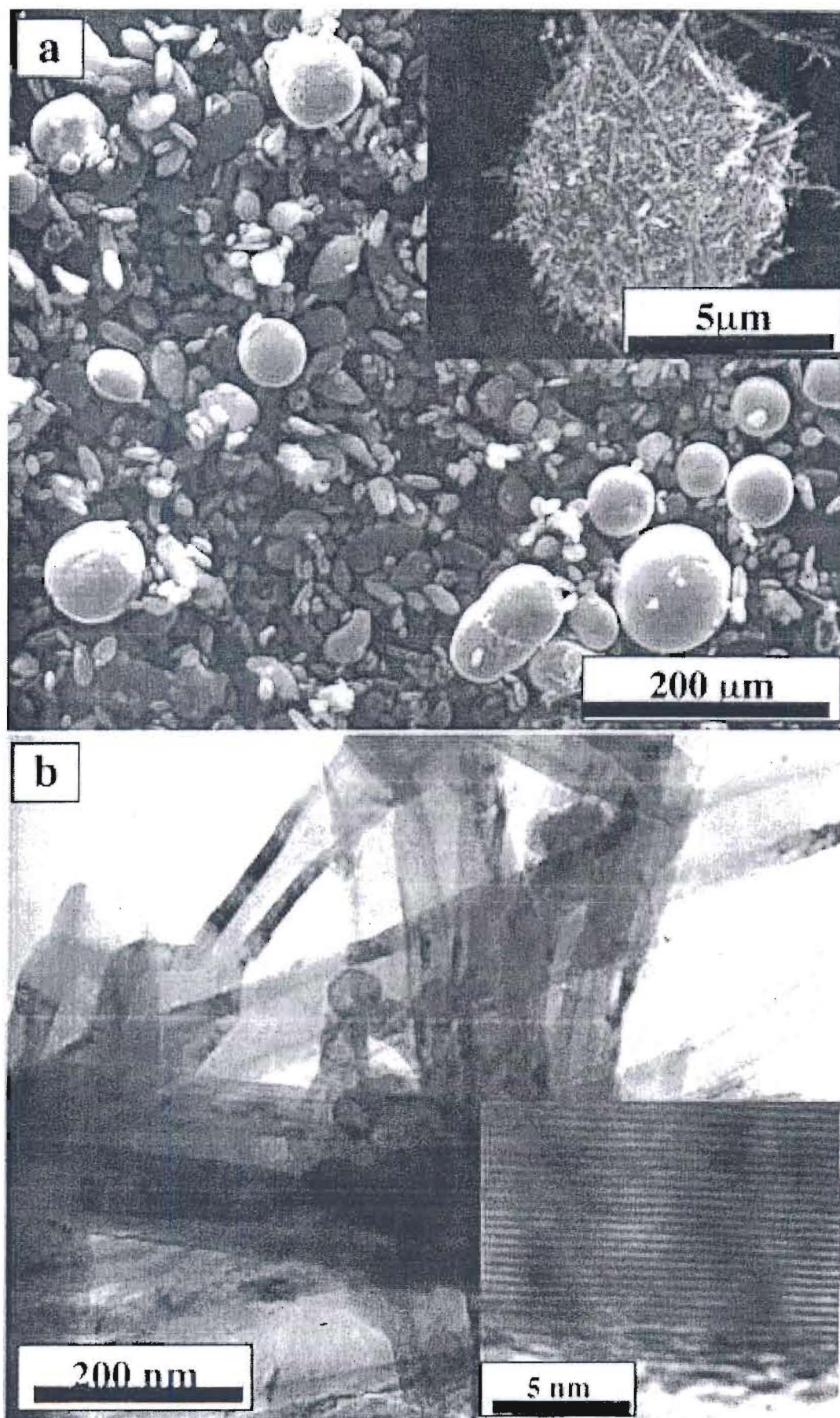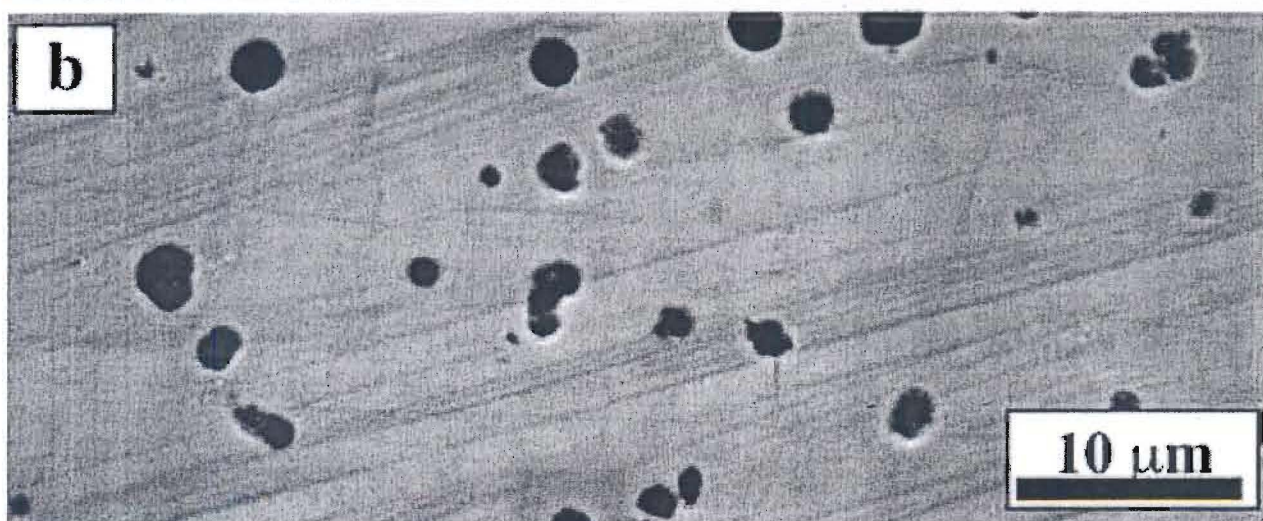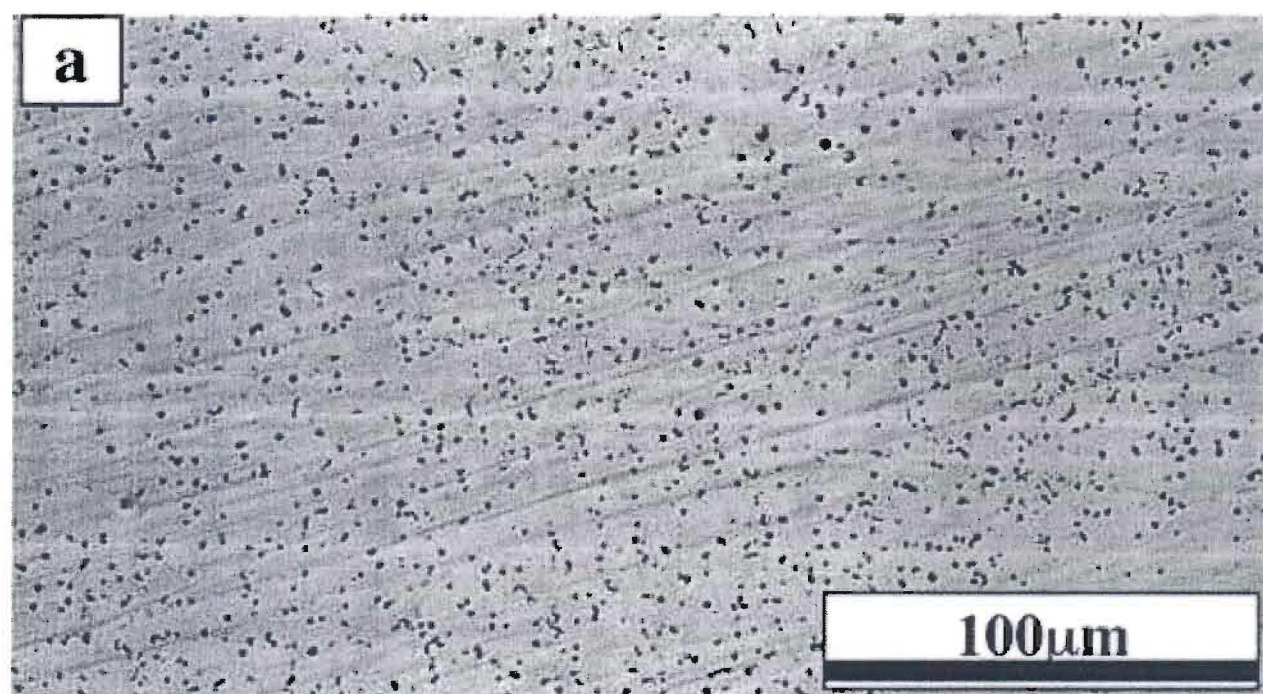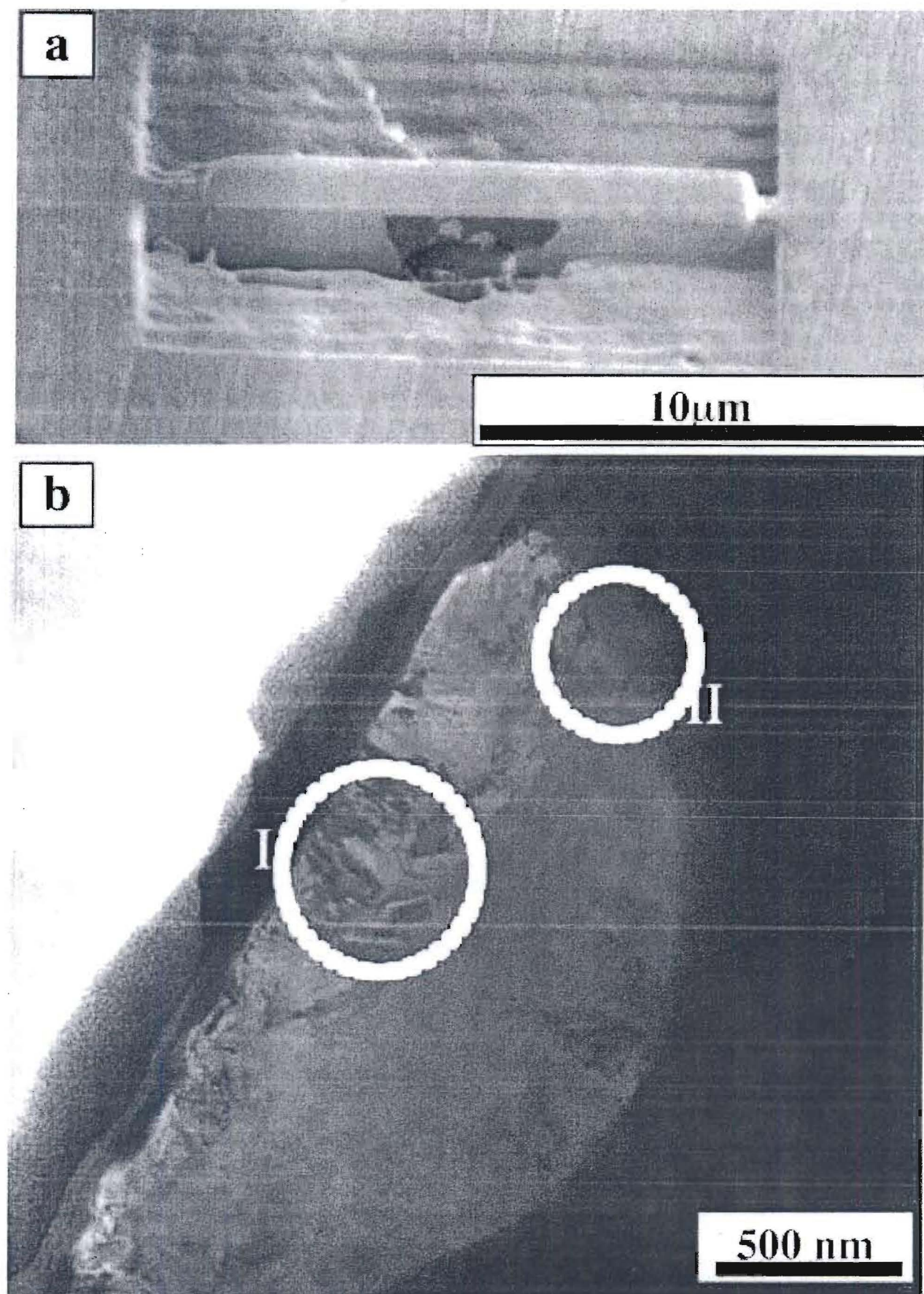Click here to download high resolution image
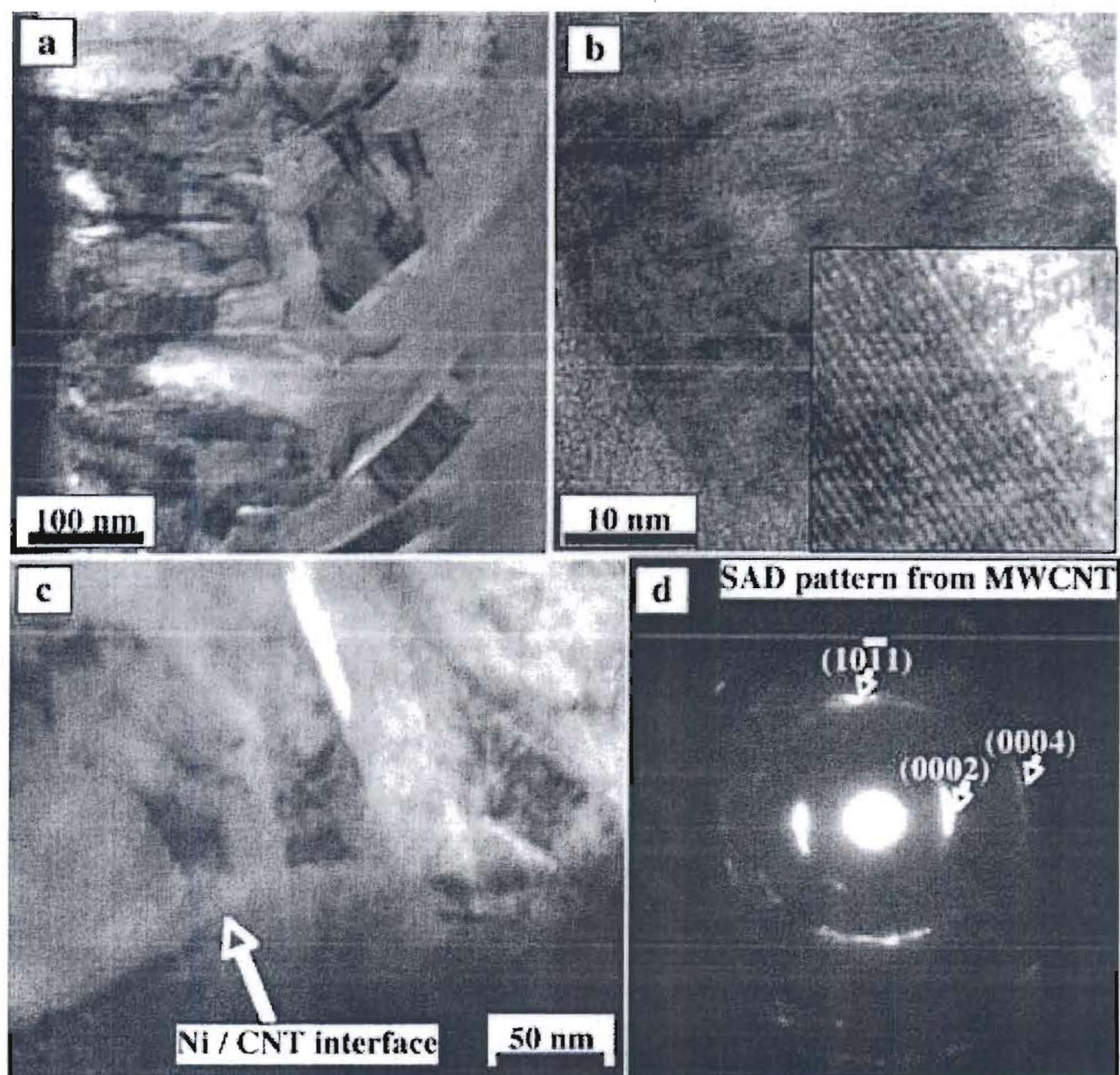
Figure 5
Click here to download high resolution image

Figure 6
Click here to download high resolution image